Mechanical twinning of monazite expels radiogenic Pb

D. Fougerouse[1,2*], S.M. Reddy[1,2], A.-M. Seydoux-Guillaume[3,4], C.L. Kirkland[1†], T.M. Erickson[1,5], D.W. Saxey[2], W.D.A. Rickard[2], D. Jacob[6], H. Leroux[6], C. Clark[1]

[1]School of Earth and Planetary Sciences, Centre for Exploration Targeting – Curtin Node[†], Curtin University, Perth, WA 6845, Australia

[2]Geoscience Atom Probe, John de Laeter Centre, Curtin University, Perth, WA 6845, Australia

[3]CNRS, Université de Lyon, UCBL, ENSL, LGL-TPE, 69622 Villeurbanne, France

[4]Univ Lyon, UJM-Saint-Etienne, F-42023 Saint-Etienne, France

[5]Jacobs – JETS, Astromaterials Research and Exploration Science division, NASA Johnson Space Center, Houston, TX, 77058, USA

[6]Univ Lille, CNRS, INRAE, Centrale Lille, UMR 8207 - UMET - Unité Matériaux et Transformations, F-59000 Lille, France.

ABSTRACT

Mechanical twins form by the simple shear of the crystal lattice during deformation In order to test the potential of narrow twins in monazite to record the timing of their formation, a ~1,700 Ma monazite grain deformed at ~980 Ma was investigated by electron backscattered diffraction (EBSD), transmission electron microscopy (TEM) and atom probe tomography (APT). APT $^{208}Pb/^{232}Th$ ages indicate that the twin was entirely reset by radiogenic Pb-loss during its formation at conditions far below the monazite closure temperature. The results are consistent with a model where Pb is liberated during rupture of REE-O bonds in the large $REEO_9$ polyhedra during twinning. Liberated Pb is likely to migrate along fast diffusion pathways such as crystal defects. The combination of a quantitative microstructural investigation and nanogeochronology provides a new approach for understanding the history of accessory phases.

INTRODUCTION

The radiogenic decay of U and Th into different isotopes of Pb provides a series of widely used geochronometers. Critical to this application is an understanding of the mobility of radiogenic Pb in minerals and how this underpins our ability to use and develop U-Th-Pb geochronology. Traditional models for Pb mobility assume temperature-dependent volume diffusion of Pb through the crystal lattice of the mineral. More recently, a number of studies have reported a relationship between trace element mobility and deformation (Fougerouse et al., 2019; Kirkland et al., 2018; Moser et al., 2009; Piazolo et al., 2012; Reddy et al., 2016; Timms et al., 2011). Pb mobility has been suggested to occur in high closure temperature minerals (zircon and monazite) during crystal-plastic deformation (Moser et al., 2009) and deformation-induced grain boundary migration (Erickson et al., 2015), with radiogenic accumulation continuing after deformation.

Deformation twinning is a common, narrow (<3 μm) microstructural feature in deformed minerals and forms by the simple shear of the crystal lattice and a highly-ordered displacement of atoms. Twinning is sensitive to temperature during deformation and strain rate, and typically is more dominant than slip at lower temperatures or at higher strain rates (Christian and Mahajan, 1995). Mechanical twinning is a deformation microstructure that has found use as a geothermometer in calcite (Ferrill et al., 2004), as a tool to determine compressive stress direction (Jamison and Spang, 1976) and has been considered a diagnostic microstructure for impact-related deformation in quartz, zircon and monazite (Erickson et al., 2016b; Goltrant et al., 1992; Moser et al., 2011; Timms et al., 2012).

In this study, we integrate electron backscattered diffraction (EBSD), transmission electron microscopy (TEM) and atom probe tomography (APT) analyses to investigate Pb mobility associated with micrometre-scale deformation twins formed within tectonically deformed monazite. We provide a framework for the analysis of mineral twins in monazite that could be further utilised in the analysis of nanoscale microstructural features in other accessory phases.

SAMPLES AND METHODOLOGY

In this contribution, we re-investigate a monazite grain from the granulite-facies rocks of the Sandmata Complex, Rajasthan, India (Fig.1), which was previously studied in detail by Erickson et al. (2015) and Fougerouse et al. (2018). Two high-temperature metamorphic events are recognised in this region, a first event at ~1720 Ma ($M1_{SC}$; ~7–10 kbar and 800–900 °C), which resulted in growth of the original monazite, and a second, fluid-absent event, at ~1000 Ma ($M2_{SC}$; ~5–7 kbar and 600–750 °C; (Buick et al., 2006)). Electron Backscatter Diffraction

(EBSD) and SIMS U/Pb analyses reveal partial Pb-loss in deformed domains of monazite and growth of neoblasts in localised deformed domains at 970 ± 14 Ma (2σ, n = 6, MSWD = 1.3; Erickson et al., 2015). Due to a spot size larger that the mechanical twins, SIMS analyses of mixed twin and host domains yield imprecise U-Pb discordant data, implying partial Pb loss in the domain analysed. These mixed domains could not be used to successfully constrain the timing of monazite deformation (Erickson et al., 2015).

EBSD analyses were used to investigate crystal lattice orientation variations and were conducted on a Tescan Mira3 scanning electron microscope equipped with a Nordlys Nano high resolution detector at Curtin University. Details of EBSD analyses are given in Erickson et al. (2015).

One atom probe specimen was prepared from a (001) twin (specimen 1) and three specimens from a neoblast (specimen 2 to 4) by focused ion beam – scanning electron microscopy (FIB-SEM; Fig. 1C). A Tescan Lyra3 Ga^{+} FIB-SEM was used to produce needle specimens and precisely select the specimen location (Rickard et al., 2020). A TEM foil was prepared with the same instrument across the boundary between the twin and the monazite host (Fig. 1C) and further thinned using a FEI Helios 600i FIB-SEM (MANUTECH USD, Saint-Etienne, France).

The TEM foil was studied using a FEI TITAN Themis 300 (University of Lille, France)to obtain high resolution high angle annular dark field (HR-HAADF) images and energy dispersive x-ray spectroscopy (EDS) with a Super-X windowless, 4 quadrant SDD detector in scanning transmission electron microscope (STEM) mode.

APT analyses were performed on at Cameca LEAP 4000X HR at the Geoscience Atom Probe facility at Curtin University (Reddy et al., 2020). The instrument was operated in laser pulsed mode with a UV laser (λ = 355 nm), laser pulse energy of 100 pJ, base temperature of 50 K and automated detection rate of 0.01 atoms per pulse. Four datasets were collected with ~8, 26, 27 and 40 million atoms, respectively. The $^{208}Pb/^{232}Th$ age was measured using the $^{208}Pb^{++}$ and $^{232}ThO^{++}$ signal and corrected following the protocol defined by Fougerouse et al. (2020). Counts were quantified by subtracting the estimated background counts from each peak. The local background level was measured from the counts in a nearby 'peak-free' range and normalised to the width of the range used for quantification (0.1 Da). The isotopic ratio uncertainties are derived from the uncertainty of each species used for calculating the ratio and reported at 95% confidence (2 sigma). The linear correlation (y = 0.381(±0.048)x – 254(±26)) between the $^{208}Pb/^{232}Th$ fractionation coefficient (y) and the $M/\Delta M_{10}$ peak parameter (x), where M is the position of the O_2^+ peak and ΔM_{10} its full-width-at-tenth-maximum, was used to correct for molecular fractionation and calculate $^{208}Pb/^{232}Th$ ages (Fougerouse et al., 2020). The error propagation of the prediction is derived from the uncertainty of the $M/\Delta M_{10}$ value, the uncertainty of the measured $^{208}Pb/^{232}ThO$ ratio and the 95% prediction band.

RESULTS

The EBSD data show that the twin is crystallographically equivalent to a 180° rotation about <100>, consistent with apparent shearing in the [100] direction on the (001) plane (e.g. Erickson et al., 2016). The observed twin dimensions in the plane of the thin section are approximately 80 μm long and 2.5 μm wide. Both the twin domain and the host monazite are relatively undeformed in the region sampled for APT with a maximum of 3.5° cumulative misorientation.

The atom probe results of specimen 1 (twin) reveal that the Ca distribution is heterogeneous within two distinct compositional domains separated by the twin boundary (Fig. 2). A proportion of the Ca within the host is clustered along with Si and Pb (~10 at.% Ca, ~1 at.% Si and ~0.7 at.% Pb) and is consistent with nanoscale inclusions of apatite in other APT studies of monazite (Fougerouse et al., 2018), whereas the twin appears homogeneous. The trace element compositions of the host and the twin are dissimilar with higher Ca and Pb in the host (1.1 vs 0.8 at.% Ca and 0.09 vs 0.05 at.% Pb, respectively) and lower Si concentration (0.04 vs 0.1 at.% Si, respectively). The twin boundary separating these two domains is enriched in Ca (2.3 at.%), Si (0.3 at.%), a weak enrichment in Pb (only visible in 3D atom maps; Fig. 2) and depleted in REEs and P.

The APT $^{208}Pb^{++}/^{232}ThO^{++}$ ratio of the host, including the cluster is 0.1789 ± 0.0058 whereas the twin domain $^{208}Pb^{++}/^{232}ThO^{++}$ ratio is 0.0965 ± 0.0057 (2 σ; Fig. 2). The peak parameter $M/\Delta M_{10}$ for this specimen is 533.8 ± 2.7. Fractionation corrected APT $^{208}Pb/^{232}Th$ ages for the host domain of specimen 1 is 1,698 ± 293 Ma (2 σ), whereas the twin domain of specimen 1 yields an age of 934 ± 193 Ma. The atom probe results from specimen 2, 3 and 4 from a single neoblast are consistent across all specimens with homogenous distribution of major and trace elements (Fig. 2 & Fig. DR1). In the neoblasts, the APT $^{208}Pb^{++}/^{232}ThO^{++}$ ratio is 0.1074 ± 0.0048 for specimen 2, 0.1117 ± 0.0056 for specimen 3 and 0.1039 ± 0.0048 for specimen 4 (Fig. 2). The peak parameter $M/\Delta M_{10}$ for Specimen 2 is 530.2 ± 1.7, 535.8 ± 1.8 for specimen 3 and 532.5 ± 1.8 for specimen 4, which yield corrected ages of 1,008 ± 198 Ma, 1,093 ± 204 Ma, and 994 ± 186 Ma, respectively (Fig. 2). The ages of the twinned domain and neoblast are within uncertainty of each other and have a weighted mean average of 1,005 ± 94 Ma (2 σ).

A HR-HAADF image across the twin boundary indicates the absence of an amorphous film and it is semi-coherent (Fig. 3B; (Ranganathan, 1966)). The STEM-EDS results are consistent with the APT findings, with enrichment in Ca and depletions in LREEs and P close to the boundary (few nm only; Fig. DR2).

AGE RESETTING AND Pb MOBILITY DURING TWIN FORMATION

The APT $^{208}Pb/^{232}Th$ ages are in good agreement with previously published SIMS and electron microprobe data for the metamorphic history of the region (Buick et al., 2006; Erickson et al., 2015). The age of the monazite host corresponds to the timing of granulite facies metamorphism which affected the region at 1,720 ± 10 Ma (Buick et al., 2006). The 1,005 ± 94 Ma weighted mean age obtained for recrystallised neoblasts and twinned domain in specimen 1 is consistent (within uncertainty) with the 970 ± 14 Ma amphibolite facies metamorphism and regional deformation event (Buick et al., 2006; Erickson et al., 2015). Therefore, all radiogenic and initial Pb was expelled from the twinned domain of the monazite crystal during the deformation event (Fig. 4).

Twin nucleation and growth have been extensively explored in the material sciences literature (Beyerlein et al., 2014; Christian and Mahajan, 1995). Mechanical twins are formed by the simple shear of the crystal lattice and the continuous movement of partial dislocations, however no studies have previously shown a relationship between twin formation and the resetting of the Th-Pb chronometer.

Three possible mechanisms can explain the resetting of the twinned domain. These include (1) dynamic recrystallization during metamorphism, (2) fluid alteration replacement, and (3)

Pb liberation during crystal shearing. The studied twin is weakly deformed (up to 3.5° of cumulative misorientation), is a single 80 μm long domain and lacks triple junctions. This observation suggests that the twin did not recrystallise after formation. We postulate that fluid-assisted recrystallization (i.e. pressure solution) did not operate during deformation of the Sandmata monazite based on the lack of a free, interconnected fluid phase in the lower crust (Yardley and Valley, 1997), coupled with textural evidence including the isolation of strain-free neoblasts within the grain interior and the absence of resetting along the exterior of the monazite (Erickson et al., 2015; Erickson et al., 2016a). In addition, high-resolution TEM data indicate that the host and the twin have a semi coherent boundary, unavailable to fluid infiltration (Fig. 3). The role of small amount of fluids (H_2O, CO_2) at the grain boundary is difficult to assess but may have facilitated the reactive transports of ions to/from the crystal surface. Therefore, we favour the third mechanism.

In monazite, Ca^{2+}, Th^{4+} and U^{4+} reside within the REE sites (Ni et al., 1995) and radiogenic Pb^{2+} is repositioned in the monazite crystal structure on the REE sites after alpha recoil during self-annealing (Seydoux-Guillaume et al., 2018; Tang et al., 2020). The monazite crystal structure is composed of an arrangement of small PO_4 tetrahedra (P-O bond lengths = 0.1524 to 0.1540 nm) and larger $REEO_9$ polyhedra (REE-O bond lengths = 0.250 to 0.277 nm). These crystal lattice parameters suggests that the PO_4 tetrahedra are more rigid compared to the $REEO_9$ polyhedra and that REE-O bonds are more likely to break than P-O bonds during twinning (Hay and Marshall, 2003). This preferential point of rupture would also affect radiogenic Pb-O and Ca-O bonds as they share the same sites, and potentially release Pb and Ca during this process (Fig. 4). The prediction of this model is that the liberation of Ca and Pb would result in a Pb-Ca-free twinned domain and the accumulation of Ca and Pb within the twin boundary. The nanogeochronology data indicate that all of the radiogenic Pb was mobilized during twin formation, while Ca composition changed by ~25%, from 1.1 at.% in the host to 0.8 at.% in the twinned domain. Ca is also highly enriched in the twin boundary (up to 2.3 at. %), whereas Pb is weakly concentrated in the same domain indicating that different mechanisms may affect Pb and Ca mobility after crystal shearing. In nine-fold coordination, the ionic radius of Pb^{2+} (1.35 Å) is larger than Ca^{2+} (1.18 Å; (Shannon, 1976)). During twinning, dislocations are necessary at the point of shearing (Cottrell and Bilby, 1951). Dislocations can trap impurities in the distorted crystal lattice surrounding the dislocation (Cottrell and Bilby, 1949), or in their cores (Johnston and Gilman, 1959). Large ions such as Pb^{2+} are likely hosted in the core of the dislocation as opposed to smaller ions such as Ca^{2+} more suited to the locally distorted lattice. Ions in dislocation cores can diffuse faster along the linear defect (Love, 1964), allowing for an efficient expulsion of Pb compared to Ca. A portion of the Ca in the Cottrell atmosphere may be reincorporated in the twinned domain as the shearing of the crystal progresses or upon subsequent thermal annealing.

No experimental data are available to constrain the temperature dependency of Pb diffusion along crystal defects, and the influence of temperature and strain rate on Pb isotopic resetting is uncertain. Nonetheless, this study demonstrates that Pb is mobilized by twin formation during deformation at 600°C. We highlight that this approach offers the potential to temporally constrain larger scale processes including, tectonic and shock driven metamorphism, that hitherto have remained elusive.

Acknowledgments

The study is supported by the Science and Industry Endowment Fund (SIEF RI13-01). The authors gratefully acknowledge support of Curtin University's Microscopy & Microanalysis Facility and the John de Laeter Centre, whose instrumentation has been supported by University, State and Commonwealth Government funding. DF acknowledges ARC funding DE190101307. We thank Ian Buick for providing the samples used in this study. Stéphanie Reynaud (Université de Saint-Etienne) is thanked for her help with FIB sample preparation of the TEM specimen. HL thanks the electron microscope facility at the University of Lille and the support of the Chevreul Institute, the European FEDER and Région Hauts-de-France. AMSG thanks CNRS INSU (TelluS-SYSTER) for financial support. We are thankful for constructive reviews by Randall Parrish and Fernando Corfu, and editorial handling by Dennis Brown.

Figure caption

Fig. 1: A) Boundary map of India; B) Simplified geological map of the Sandmata granulite complex with location of sample, modified from Buick et al. (2010). AS: Aravalli Supergroup; BGC: Banded Gneiss Complex; DS: Delhi Supergroup; C) Crystallographic orientation EBSD

map. Grain Reference Orientation Deviation (GROD) up to 15° on a green colour scale; Twins are colour coded red for misorientation ranging between 0 and 20° from the reference point "+"; modified from Erickson et al. (2015). The atom probe Tomography (APT) samples were extracted from a (100) twin (specimen 1) and one neoblast (specimen 2, 3 and 4); D) Lower hemisphere, equal area projection at site of atom probe specimen 1. The green symbols represent the monazite host and the red symbols the twin domain.

Fig. 2: A) Reconstructed three-dimensional atom probe image of Ca, Si and ^{208}Pb distribution for specimen 1 (twin + host) and specimen 2 (neoblast). Each sphere represents one atom. The twinned domain is marked by a homogeneous Ca, Si and Pb distribution whereas the host is heterogeneous with apatite nano-inclusions. The neoblast Ca, Si and Pb distribution is homogeneous. B) Nanoscale ^{208}Pb/^{232}Th age data. The ages are colour coded by grain domains (Green: host; Blue: neoblast; Orange: twin). The host monazite is consistent with the granulite metamorphism whereas the neoblast and twin data with deformation associated with amphibolite metamorphism.

Fig. 3: A) HR-HAADF image of the twin boundary showing the absence of amorphous material within the boundary. C) Indexed Fourier Transform of a square area on the right side of image B and the structure model seen along the [010] orientation. Only the heavy REE atoms are seen on the HR-HAADF image.

Fig. 4: Schematic model of the age resetting of the twin during its formation. Diagram not at scale.

References

Beyerlein, I. J., Zhang, X., and Misra, A., 2014, Growth twins and deformation twins in metals: Annual Review of Materials Research, v. 44, p. 329-363.

Buick, I., Allen, C., Pandit, M., Rubatto, D., and Hermann, J., 2006, The Proterozoic magmatic and metamorphic history of the Banded Gneiss Complex, central Rajasthan, India: LA-ICP-MS U–Pb zircon constraints: Precambrian Research, v. 151, no. 1, p. 119-142.

Christian, J. W., and Mahajan, S., 1995, Deformation twinning: Progress in materials science, v. 39, no. 1-2, p. 1-157.

Cottrell, A., and Bilby, B., 1951, LX. A mechanism for the growth of deformation twins in crystals: The London, Edinburgh, and Dublin Philosophical Magazine and Journal of Science, v. 42, no. 329, p. 573-581.

Cottrell, A. H., and Bilby, B., 1949, Dislocation theory of yielding and strain ageing of iron: Proceedings of the Physical Society. Section A, v. 62, no. 1, p. 49.

Erickson, T., Pearce, M., Taylor, R., Timms, N. E., Clark, C., Reddy, S., and Buick, I., 2015, Deformed monazite yields high-temperature tectonic ages: Geology, v. 43, no. 5, p. 383-386.

Erickson, T., Reddy, S., Timms, N., Pearce, M., Taylor, R., Clark, C., and Buick, I., 2016a, Deformed monazite yields high-temperature tectonic ages: REPLY: Geology, v. 44, no. 1, p. e378-e378.

Erickson, T. M., Cavosie, A. J., Pearce, M. A., Timms, N. E., and Reddy, S. M., 2016b, Empirical constraints on shock features in monazite using shocked zircon inclusions: Geology, v. 44, no. 8, p. 635-638.

Ferrill, D. A., Morris, A. P., Evans, M. A., Burkhard, M., Groshong Jr, R. H., and Onasch, C. M., 2004, Calcite twin morphology: a low-temperature deformation geothermometer: Journal of structural Geology, v. 26, no. 8, p. 1521-1529.

Fougerouse, D., Kirkland, C. L., Saxey, D. W., Seydoux-Guillaume, A. M., Rowles, M. R., Rickard, W. D. A., and Reddy, S. M., 2020, Nanoscale isotopic dating of monazite: Geostandards and Geoanalytical Research, v. in press.

Fougerouse, D., Reddy, S. M., Kirkland, C. L., Saxey, D. W., Rickard, W. D., and Hough, R. M., 2019, Time-resolved, defect-hosted, trace element mobility in deformed Witwatersrand pyrite: Geoscience Frontiers, v. 10, no. 1, p. 55-63.

Fougerouse, D., Reddy, S. M., Saxey, D. W., Erickson, T. M., Kirkland, C. L., Rickard, W. D. A., Seydoux-Guillaume, A. M., Clark, C., and Buick, I. S., 2018, Nanoscale distribution of Pb in monazite revealed by atom probe microscopy: Chemical Geology, v. 479, p. 251-258.

Goltrant, O., Leroux, H., Doukhan, J.-C., and Cordier, P., 1992, Formation mechanisms of planar deformation features in naturally shocked quartz: Physics of the Earth and Planetary Interiors, v. 74, no. 3-4, p. 219-240.

Hay, R., and Marshall, D., 2003, Deformation twinning in monazite: Acta Materialia, v. 51, no. 18, p. 5235-5254.

Jamison, W. R., and Spang, J. H., 1976, Use of calcite twin lamellae to infer differential stress: Geological Society of America Bulletin, v. 87, no. 6, p. 868-872.

Johnston, W., and Gilman, J. J., 1959, Dislocation velocities, dislocation densities, and plastic flow in lithium fluoride crystals: Journal of Applied Physics, v. 30, no. 2, p. 129-144.

Kirkland, C. L., Fougerouse, D., Reddy, S. M., Hollis, J., and Saxey, D. W., 2018, Assessing the mechanisms of common Pb incorporation into titanite: Chemical Geology, v. 483, p. 558-566.

Love, G., 1964, Dislocation pipe diffusion: Acta Metallurgica, v. 12, no. 6, p. 731-737.

Moser, D., Cupelli, C., Barker, I., Flowers, R., Bowman, J., Wooden, J., and Hart, J., 2011, New zircon shock phenomena and their use for dating and reconstruction of large impact structures revealed by electron nanobeam (EBSD, CL, EDS) and isotopic U–Pb and (U–Th)/He analysis of the Vredefort dome: Canadian Journal of Earth Sciences, v. 48, no. 2, p. 117-139.

Moser, D., Davis, W., Reddy, S., Flemming, R., and Hart, R., 2009, Zircon U–Pb strain chronometry reveals deep impact-triggered flow: Earth and Planetary Science Letters, v. 277, no. 1, p. 73-79.

Ni, Y., Hughes, J. M., and Mariano, A. N., 1995, Crystal chemistry of the monazite and xenotime structures: American Mineralogist, v. 80, no. 1, p. 21-26.

Piazolo, S., Austrheim, H., and Whitehouse, M., 2012, Brittle-ductile microfabrics in naturally deformed zircon: Deformation mechanisms and consequences for U-Pb dating: American Mineralogist, v. 97, no. 10, p. 1544-1563.

Ranganathan, S., 1966, On the geometry of coincidence-site lattices: Acta Crystallographica, v. 21, no. 2, p. 197-199.

Reddy, S. M., Saxey, D. W., Rickard, W. D. A., Fougerouse, D., Montalvo, S. D., Verberne, R., and van Riessen, A., 2020, Atom Probe Tomography: Development and Application to the Geosciences: Geostandards and Geoanalytical Research, v. 44, no. 1, p. 5-50.

Reddy, S. M., van Riessen, A., Saxey, D. W., Johnson, T. E., Rickard, W. D., Fougerouse, D., Fischer, S., Prosa, T. J., Rice, K. P., and Reinhard, D. A., 2016, Mechanisms of deformation-induced trace element migration in zircon resolved by atom probe and correlative microscopy: Geochimica et Cosmochimica Acta, v. 195, p. 158-170.

Rickard, W. D., Reddy, S. M., Saxey, D. W., Fougerouse, D., Timms, N. E., Daly, L., Peterman, E., Cavosie, A. J., and Jourdan, F., 2020, Novel Applications of FIB-SEM-Based ToF-SIMS in Atom Probe Tomography Workflows: Microscopy and Microanalysis, p. 1-8.

Seydoux-Guillaume, A.-M., Deschanels, X., Baumier, C., Neumeier, S., Weber, W. J., and Peuget, S., 2018, Why natural monazite never becomes amorphous: Experimental evidence for alpha self-healing: American Mineralogist, v. 103, no. 5, p. 824-827.

Shannon, R. D., 1976, Revised effective ionic radii and systematic studies of interatomic distances in halides and chalcogenides: Acta crystallographica section A: crystal physics, diffraction, theoretical and general crystallography, v. 32, no. 5, p. 751-767.

Tang, X., Li, Q.-L., Zhang, B., Wang, P., Gu, L.-X., Ling, X.-X., Fei, C.-H., and Li, J.-H., 2020, The Chemical State and Occupancy of Radiogenic Pb, and Crystallinity of RW-1 Monazite Revealed by XPS and TEM: Minerals, v. 10, no. 6, p. 504.

Timms, N. E., Kinny, P. D., Reddy, S. M., Evans, K., Clark, C., and Healy, D., 2011, Relationship among titanium, rare earth elements, U-Pb ages and deformation microstructures in zircon: Implications for Ti-in-zircon thermometry: Chemical Geology, v. 280, no. 1-2, p. 33-46.

Timms, N. E., Reddy, S. M., Healy, D., Nemchin, A. A., Grange, M. L., Pidgeon, R. T., and Hart, R., 2012, Resolution of impact-related microstructures in lunar zircon: A shock-

deformation mechanism map: Meteoritics & Planetary Science, v. 47, no. 1, p. 120-141.
Yardley, B. W., and Valley, J. W., 1997, The petrologic case for a dry lower crust: Journal of Geophysical Research: Solid Earth, v. 102, no. B6, p. 12173-12185.

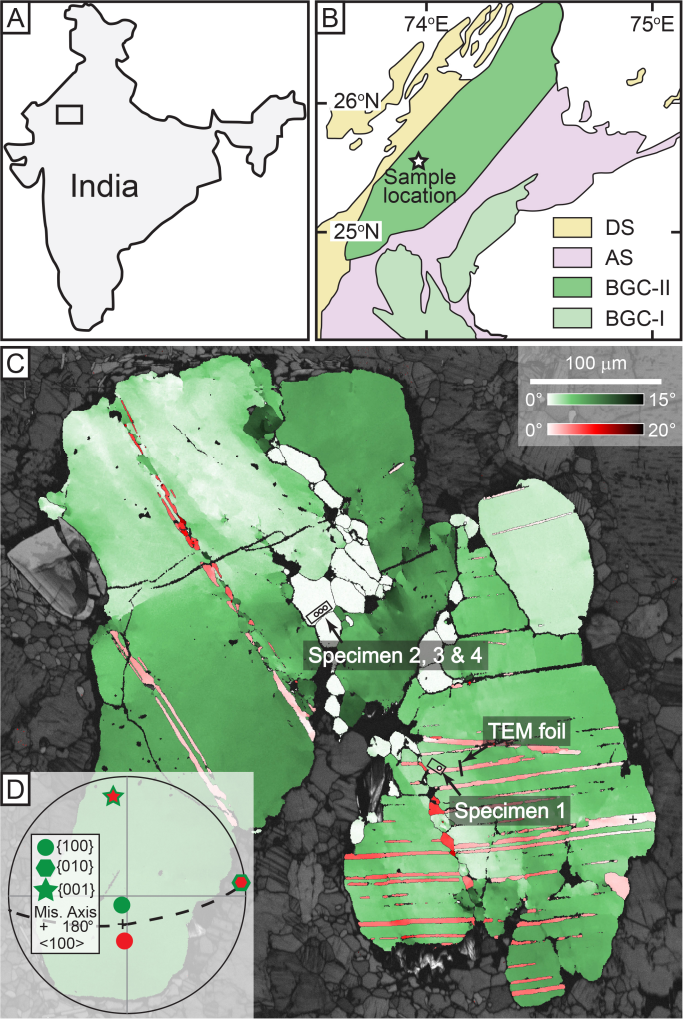

A
India
B
74°E
75°E
26°N
25°N
Sample location
DS
AS
BGC-II
BGC-I
C
100 μm
0°
15°
0°
20°
Specimen 2, 3 & 4
TEM foil
Specimen 1
D
{100}
{010}
{001}
Mis. Axis
+ 180°
<100>

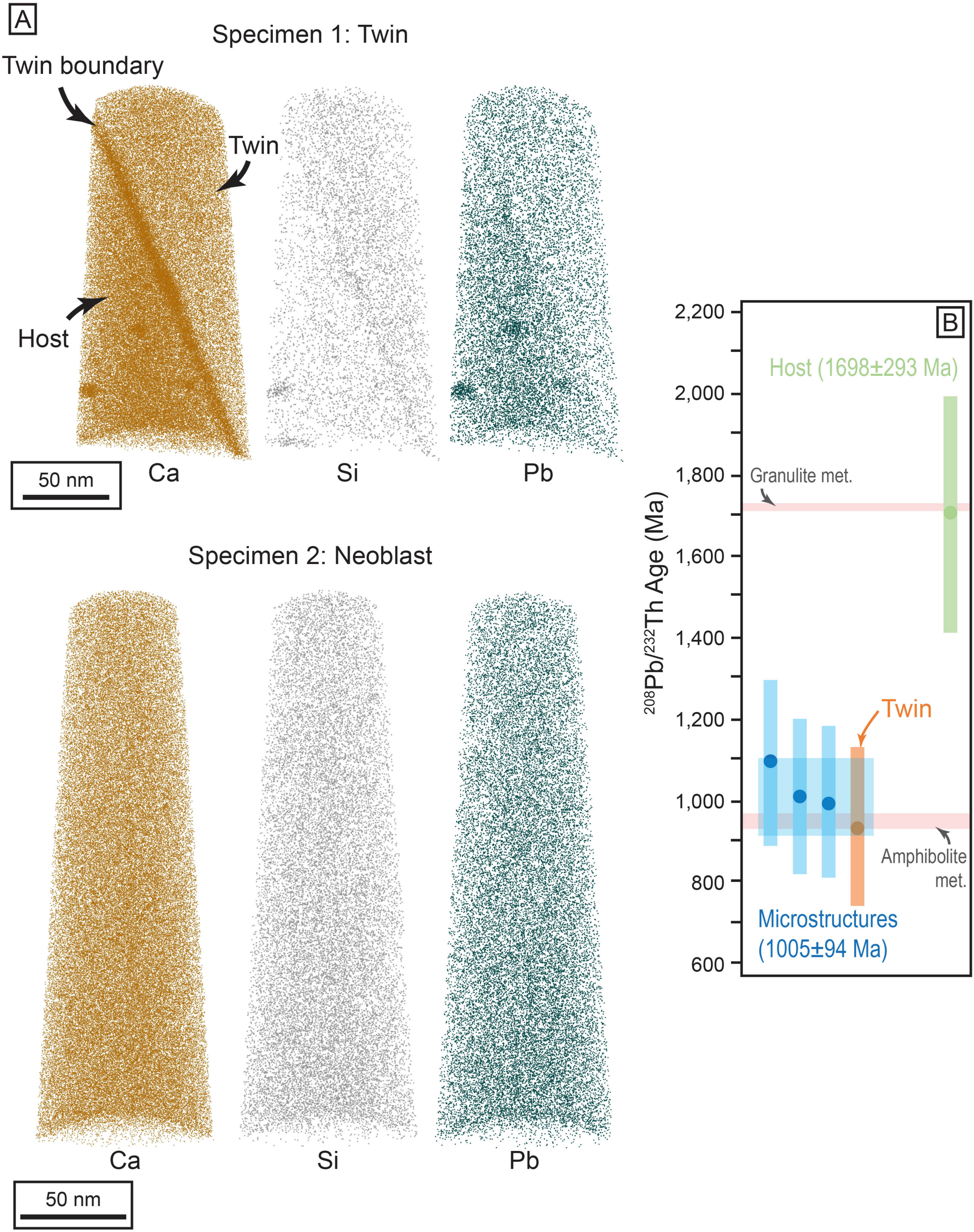
A
Specimen 1: Twin
Twin boundary
Twin
Host
Ca
Si
Pb
50 nm
Specimen 2: Neoblast
Ca
Si
Pb
50 nm
B
Host (1698±293 Ma)
Granulite met.
Twin
Amphibolite met.
Microstructures (1005±94 Ma)
^{208}Pb/^{232}Th Age (Ma)
2,200
2,000
1,800
1,600
1,400
1,200
1,000
800
600

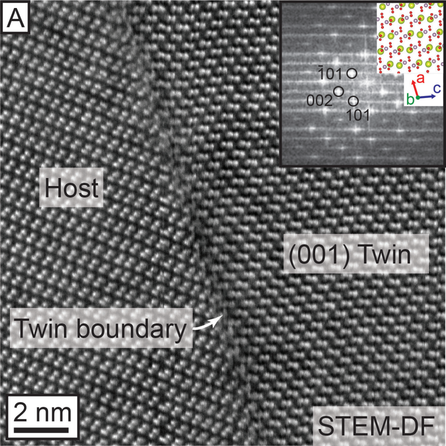
A
$\bar{1}01$
002
101
a
b
c
Host
(001) Twin
Twin boundary
2 nm
STEM-DF

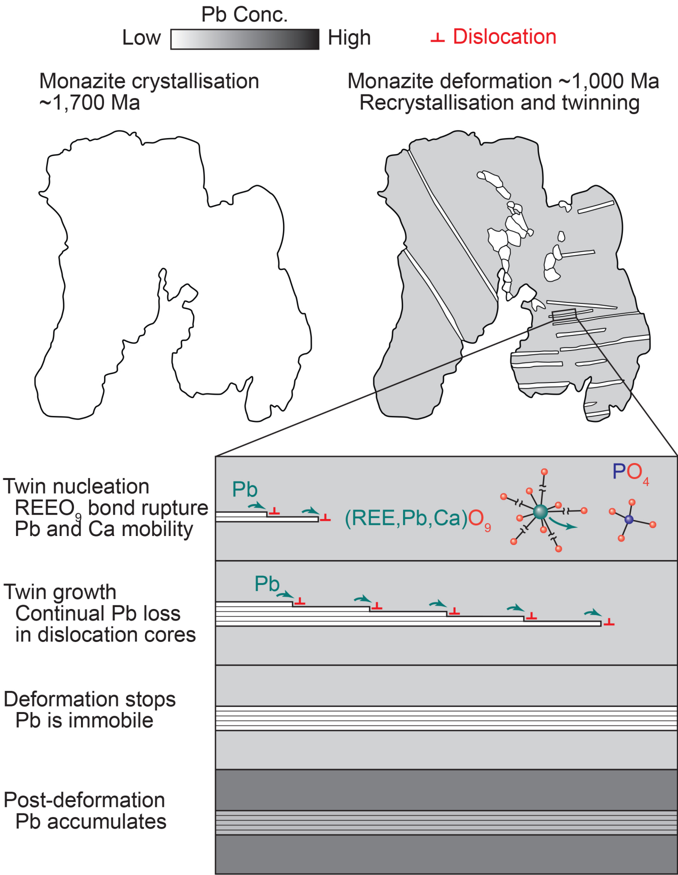
Pb Conc.
Low
High
⊥ Dislocation
Monazite crystallisation ~1,700 Ma
Monazite deformation ~1,000 Ma
Recrystallisation and twinning
Twin nucleation
REEO$_9$ bond rupture
Pb and Ca mobility
Pb
(REE,Pb,Ca)O$_9$
PO$_4$
Twin growth
Continual Pb loss in dislocation cores
Pb
Deformation stops
Pb is immobile
Post-deformation
Pb accumulates